2 Phase 1: Rate determining step during solid state reduction

2.1 Solid state reduction in a mixed bed: Theoretical aspects

2.1.1 Basic reactions and thermodynamic considerations

When a composite material mixture (such as the material mixture fed into a rotary kiln- or Ifcon process) heats up to temperatures in excess of 100°C, drying of the mixture occurs and devolatilization of the coal[20] is initiated. Once the temperature of the material increases beyond 300°C, the rate of devolatilization increases significantly[21,22]. Devolatilization products (such as CO and H_2) initiate reduction of iron oxides[23], according to the following reaction:

$$Fe_xO_y\ (s) + CO\ (\text{or } H_2)(g) \Rightarrow Fe_xO_{y-1}\ (s\ ) + CO_2\ (\text{or } (H_2O)(g) \qquad (2.a)$$

At temperatures above 306°C[14] calcination of the magnesite component of the dolomite occurs according to the following reaction:

$$MgCO_3(s) \Rightarrow MgO(s) + CO_2(g) \qquad (2.b)$$

As the material is heated to temperatures in excess of 700°C[14] the carbon gasification (or Boudouard) reaction sets in, and reduction of the iron oxides with CO proceeds [7,14].

$$CO_2(g) + C(s) \Rightarrow 2CO(g) \qquad (2.c)$$

In addition to the Boudouard reaction, carbon can also be gasified by water vapour to produce hydrogen gas. This reaction, which is called the water-gas reaction, is shown below.

$$H_2O(g) + C(s) \Rightarrow CO(g) + H_2\ (g) \qquad (2.d)$$

(This part of the study aims to test whether the hydrogen produced, contribute to the reduction reaction).

At temperatures above 895°C calcination of calcite (limestone) occurs according to the following reaction[14].

$$CaCO_3(s) \Rightarrow CaO(s) + CO_2(g) \quad (2.e)$$

Note that the overall reduction reaction (when combining ***equations 2.a*** and ***2.c***) is as follows:

$$Fe_xO_y\ (s) + C(s) \Rightarrow Fe_xO_{y-1}\ (s\ ) + CO\ (g) \quad (2.f)$$

To study the various reduction steps, ***equation 2.a*** can be subdivided into the following equations:

Reduction of hematite with carbon monoxide (or hydrogen):

$$3Fe_2O_3(s) + CO(\text{or } H_2)(g) \Rightarrow 2Fe_3O_4(s) + CO_2(\text{or } H_2O)(g) \quad (2.g)$$

Reduction of magnetite with carbon monoxide (or hydrogen) below 564°C:

$$Fe_3O_4(s) + CO(\text{or } H_2)(g) \Rightarrow 3Fe(s) + CO_2(\text{or } H_2O)\ (g) \quad (2.h)$$

Reduction of magnetite with carbon monoxide (or hydrogen) above 564°C:

$$Fe_3O_4(s) + CO(\text{or } H_2)(g) \Rightarrow 3FeO(s) + CO_2(\text{or } H_2O)\ (g) \quad (2.i)$$

Reduction of wustite with carbon monoxide (or hydrogen):

$$FeO(s) + CO(\text{or } H_2)(g) \Rightarrow Fe(s) + CO_2(\text{or } H_2O)\ (g) \quad (2.j)$$

From the thermodynamic data of Kubaschewski et al[14], the equilibrium iron oxide diagram (in a CO/CO_2 atmosphere) and carbon stability diagram[7] is constructed (as shown in ***Figure 9***). The equilibrium iron oxide diagram (in a H_2/H_2O atmosphere) [7] is shown in ***Figure 10***.

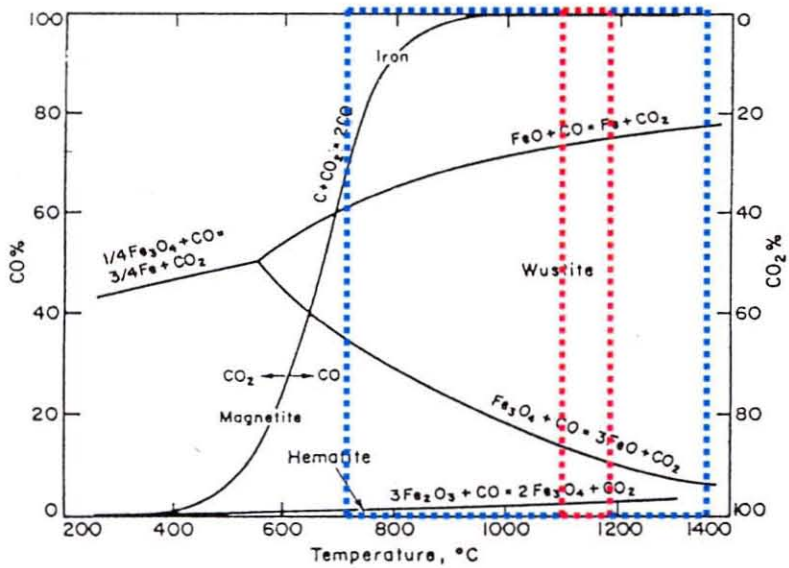

Figure 9: *Equilibrium iron oxide- and carbon stability diagrams in a CO/CO_2 atmosphere[7]. The anticipated operational window for the solids bed in the Ifcon process is shown as a blue rectangle. The operational window where tests regarding the first phase of the investigation were done is indicated with a red rectangle.*

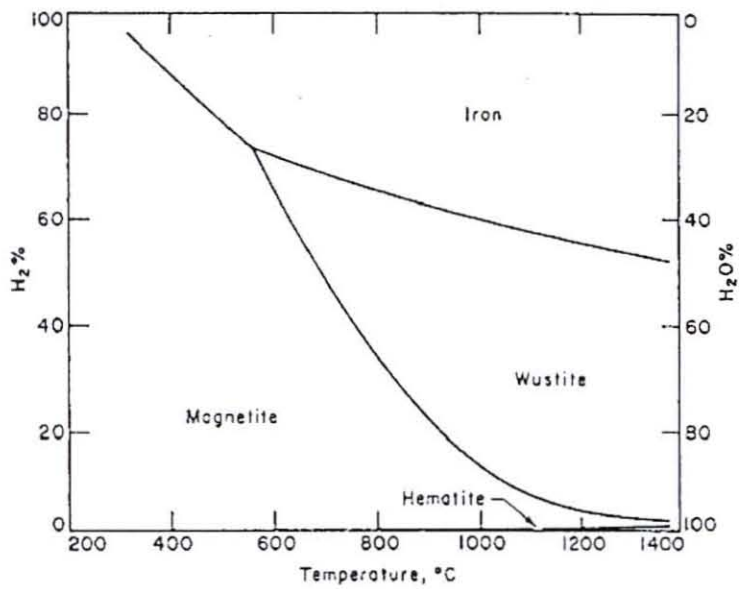

Figure 10: *Equilibrium iron oxide diagram in a H_2/H_2O atmosphere[7].*

Figure 9 shows the extent to which reduction of iron oxide with CO, and the oxidation of carbon with CO_2, will tend to proceed, while ***Figure 10*** shows the extent to which reduction of iron oxide will tend to proceed with H_2 under specific conditions. These diagrams also indicate the stable phases that will be present at a specific temperature and gas composition (with $p_{CO} + p_{CO_2} = 1$ for ***Figure 9*** and $p_{H_2} + p_{H_2O} = 1$ for ***Figure 10***). Accordingly, at typical temperatures between 700°C and 1400°C (in the solids bed of the Ifcon process) and anticipated CO/CO_2 ratios of 0.5 to 1.0[15], the stable oxide phases will be wustite and iron.

2.1.2 Reaction mechanisms and rate controlling steps

To investigate the rate at which reactions occur, the reaction mechanisms must be considered. According to the overall reduction reaction ***(2.f)***, iron oxide in the ore is reduced by solid carbon to produce metallic iron and CO gas.

Although the overall reaction is between iron oxide and carbon, literature shows that reduction predominantly occur via intermediate CO gas, rather than by direct contact between iron oxide and carbon[7,23,24]. The reduction mechanism for reduction occurring via intermediate CO gas is schematically shown in ***Figure 11***.

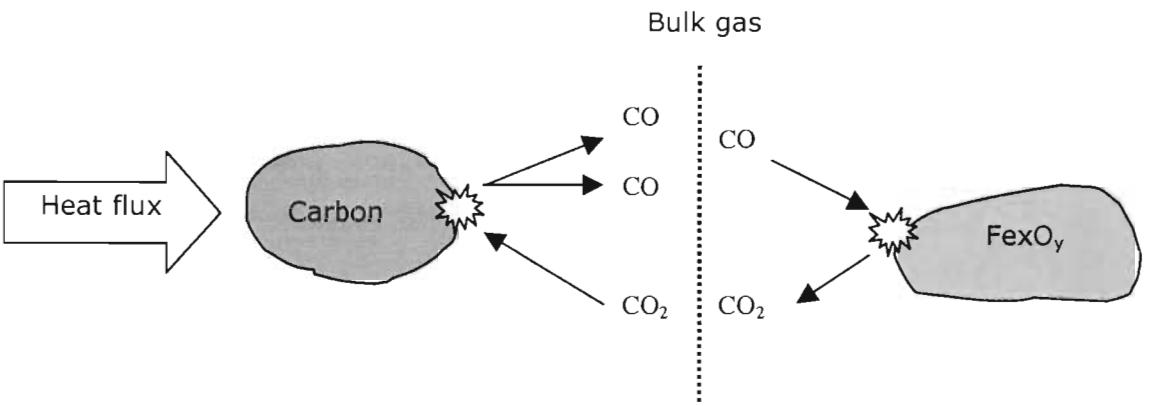

Figure 11: *Schematic representation of solid-state reduction via CO as intermediate gas.*

Figure 11 shows that reduction is performed by the gaseous species CO, while the product gas (CO_2) is regenerated by the Boudouard reaction to carbon monoxide, which in turn reacts with the iron-ore specie. Note that the average composition of the gas, which evolves from such an ore-carbon mixture, will depend on the relative rates of the reduction and Boudouard reactions. The same argument also holds when reduction is achieved with H_2 while the product gas (H_2O) is regenerated by the water-gas reaction.

The individual reaction steps by which the overall reaction (presented in ***Figure 11***) proceeds are[7,24]:

a. Diffusion of CO from the bulk gas to the iron oxide particle.
b. Diffusion of CO inward through the reduced product layer.
c. Chemical reduction reaction of iron oxide with CO gas.
d. Diffusion of CO_2 outwards through the reduced product layer.
e. Diffusion of CO_2 from the iron/iron oxide particle to the bulk gas.
f. Diffusion of CO_2 from the bulk gas to the carbon particle.
g. Heat transfer to the carbon particle.
h. Chemical oxidation of carbon with CO_2.
i. Diffusion of CO from the carbon particle to the bulk gas.

In order to quantify the rate of the overall reaction, each reaction step must be quantified, or eliminated (as not being rate controlling). (This is finalised in the second phase of this investigation.)

Of the above steps, a, e, f and i are **mass transfer** steps, and their rates can be described by equations such as ***(2.k).*** If any one of these steps governs the rate of the overall reaction, the reaction is mass transfer controlled.

The rate of mass transfer between the bulk of a phase and the interface with another phase can be quantified with the following equation:

$$J = m(C_{bulk}-C_{interface}) \qquad (2.k)$$

where, *J* (with units: $mol.m^{-2}.s^{-1}$) is the flux of the given species towards an interface, *m* (with units: $m.s^{-1}$) is the mass transfer coefficient, and *C* (with units: $mol.m^{-3}$) is the concentration of the species.

Steps b and d are **diffusion** steps[25,26], and their rates can be described by equations such as ***(2.l).*** If diffusion governs the rate of the overall reaction, the reaction is referred to as diffusion controlled.

The rate of diffusion transfer between the surface of a particle and the reaction interface or site where the actual chemical reaction takes place, can be quantified with the following equation[27]:

$$J = D\left(\frac{C_{\text{particle surface}} - C_{\text{reaction interface}}}{dx}\right) \qquad (2.l)$$

where J (with units: $mol.m^{-2}.s^{-1}$) is the flux of the given species towards an interface, *D* (with units: $m^2.s^{-1}$) is the diffusivity, $C_{particle\ surface}$ *and* $C_{reaction\ interface}$ (with units: $mol.m^{-3}$) are the concentration of the species on the particle surface and reaction interface respectively and *dx* (with unit: m) is the product layer thickness or distance over which the concentration gradient exists.

Steps c, and h are chemical reactions, and their rates are described by equations such as ***(2.m)***[28]. If the rate of the overall reaction is governed by the rate of either of the chemical reactions, the rate at which the chemical reactions occur must be quantified.

For the general reaction

$$bB + cC \quad \Leftrightarrow \quad dD + eE$$

where b, c, d, and e are stoichiometric coefficients of reagents B, C, D and E respectively, the rate of the reaction is typically given by the following rate expression:[28]:

$$J = k\left[\left(a_B^b \times a_C^c\right)_{\text{int erface}} - \left(a_B^b \times a_C^c\right)_{equilibrium}\right] \qquad (2.m)$$

where J (with units $mol.m^{-2}.s^{-1}$) is the flux of one of the species (*B, C, D* or *E*) to or away from the interface, a_i is the activity of species i, and k is the reaction rate constant.

If the gasification and reduction reactions have similar rates, they both would be controlling. This implies that neither of the two reactions would be at their equilibrium values, but that a quasi-equilibrium would be established, somewhere between these two equilibrium values.

When two of the above rate mechanisms (mass transfer, diffusion transfer or chemical reaction rate) influence the rate of reduction, the overall mechanism is referred to as "mixed control"[7].

Steps g is a heat transfer steps, and it's rate can be described by the rate of conduction-, convection- or radiation heat-transfer. If the rate of the overall reaction is governed by the rate of either of these steps, the overall reaction is heat transfer controlled. Heat transfer control therefore occurs when heat for the reactions is supplied at a slower rate than the rate at which the reactions consume the heat. The rate of heat transfer depends on the heat transfer mechanism (i.e. conduction, convection or radiation), which is influenced by the configuration of the material (e.g. packed bed or fluidised bed). The rates of heat transfer are mathematically expressed in ***(2.n)*** to ***(2.p)***[29].

General rate expression for conduction heat transfer:

$$q = k\,A\left(\frac{T_{heat\ source} - T_{particle}}{dx}\right) \qquad (2.n)$$

General rate expression for convection heat transfer:

$$q = h\,A\left(T_{heat\ source} - T_{particle}\right) \qquad (2.o)$$

General rate expression for thermal radiation heat transfer:

$$q = F_{\varepsilon}\,F_{G}\,\sigma\,A\left(T^{4}_{heat\ source} - T^{4}_{particle}\right) \qquad (2.p)$$

In these equations, q is the heat flux (with units: $W.m^{-2}$), A is the area through which the heat flux is transferred (with unit: m^2), $T_{heat\ source}$ and $T_{particle}$ are the temperatures of the heat source and particle respectively (with units: K), k and h are the thermal conductivity and convection heat transfer coefficients respectively, F_ε is the emissivity function, F_G is the geometric "view factor" function and σ is the Stefan-Boltzmann constant (with a value of $5.669 \times 10^{-8}\ W.m^2.K^4$).

2.1.3 Relevant studies

Various studies investigated the mechanisms and rate-determining steps during reduction of composite iron ore-reductant mixtures (with graphite, coke, coal char and coal used as reductant). During these investigations, the analyses of product gas, the influence of reductant content and particle size, and the magnitude of the apparent activation energy were used to evaluate the rate-determining step during reduction. Most authors concluded that the rate of the gasification reaction governed the overall rate of the reaction[30].

2.1.3.1 Carbon gassification

For the reduction of ore-coal mixtures, Bryk and Lu[24] noted that the overall reduction rate is controlled by the oxidation of carbon at temperatures below 1100°C, while at higher temperatures the reaction rate is controlled by a combination of the reduction and Boudouard reactions. They also found that when small coal particles were used (<150µm), changes to the particle size did not influence the degree of metallization achieved in 15 minutes, but increasing the coal size beyond 150µm decreased the metallization rate.

Shivaramakrishna[31], who reacted composite pellets in a bed of coal between 950°C and 1050°C, concluded that the Boudouard reaction governed the overall reduction reaction. Note that the Boudouard reaction is highly endothermic and may be limited by heat transfer limitations.

Fruehan[32] showed that the reactivity of different carbon sources differs from one another. Different authors used different types of carbon sources including coconut charcoal, coal char, petroleum coke, and graphite, but a clear correlation between activation energy and type of carbon was not found[33,34,35].

The activation energies for gasification of carbon with CO_2 mostly ranged from 215 to 310 kJ/mol[30], while the activation energies for gasification of carbon with steam ranged from 120 to 245 kJ/mol[30].

2.1.3.2 Reduction reaction

Srinivasan and Lahiri[36] measured the CO/CO_2 ratio of the product gas when composite pellets were reacted. They found that the CO/CO_2 ratio decreased with decreasing carbon content of the pellet, thereby changing the rate controlling reaction from carbon gasification to wustite reduction.

Reported activation energies for reduction of FeO with CO usually ranged from 116kJ/mol to 151 kJ/mol[37], while the activation energies for reduction of Fe_2O_3 and FeO with H_2 was mostly reported as 64-74 kJ/mol and 52-77kJ/mol respectively[30].

Sun and Lu[38] developed a mathematical model to describe the non-isothermal reduction of magnetite-coal mixtures. For reduction with CO and H_2, they found activation energy values in the ranges 65 - 74 kJ/mol, and 61 – 69 kJ/mol respectively.

2.1.3.3 Temperature and Heat transfer

Bryk and Lu[24] reacted large masses of ore-coal mixtures at 900°C, 1100°C and 1300°C. From their results, they concluded that heat transfer to the sample as well as conduction within the sample affected the reaction kinetics significantly.

Huang and Lu[23] reacted ore–coal mixtures at 1200°C in a muffle furnace. Their results suggested that heat transfer limited the kinetics of their system, due to the heat demand from endothermic reactions occurring in the mixture.

In an experiment, similar to that of Huang and Lu, Sun and Lu[39,40] found that heat transfer to, as well as conduction within, the material mixture was rate limiting due to the endothermic nature of the reactions. They also concluded that heat transfer within the solids bed was mainly due to conduction, rather than convection or radiation, for furnace temperatures below 1300°C

Wang *et al.*[41] inferred from heat transfer and kinetic calculations that, during fast heating, reduction rate of composite pellets is initially controlled by the chemical reduction reaction, where after the rate is controlled by heat transfer.

2.1.3.4 The influence of volatiles

Wang *et al.*[42] reduced composite ore-coal pellets and noted that significant devolatilisation only started at 400°C. They also found that volatiles significantly influence the rate of reduction at temperatures above 700°C. Similar results were also obtained by Dutta and Gosh[43], Dey *et al.*[44], and Shivaramakrishna *et al.*[31] Dutta and Gosh proposed an explanation for the reactions occurring, and noted that devolatilisation of coal in an iron-coal mixture is different to devolatilisation of unmixed coal.

Sun and Lu[39], Sharma[45], Huang and Lu[23] and Bryk and Lu[24] all observed some contribution of volatiles to the reduction of iron ore in a packed bed. Bryk and Lu[24] showed that when coal was replaced with graphite, the rate of metallization of iron ore composites at 1150°C decreased.

Coetsee *et al.*[30] modelled the reduction of magnetite-coal pellets, and predicted that volatile matter contribute to reduction of pellets.

2.2 Experimental aspects

A thermo gravimetric study was done to investigate the influence of changes to feed material characteristics and exposure temperature, on the reduction rate of composite material mixtures. The experimental apparatus mainly comprised of a high temperature tube furnace and associated gas flow rate control system.

2.2.1 Experimental apparatus

2.2.1.1 High temperature furnace.

The tests were performed in a vertical tube resistance furnace. A mullite tube (one end closed) of 60mm inside and 70mm outside diameter, served as work tube. The furnace was heated by eight silicon carbide heating elements and the furnace was equipped with a PID (proportional integral derivative) controller, for furnace temperature control. A schematic representation of the furnace arrangements is shown in ***Figure 12***.

A water-cooled brass ring was fitted onto the open end of the work tube. The interface between the brass ring and the work tube was made gas tight with two rubber O-rings and vacuum grease.

Purge gas entered the work tube, through an alumina tube (that extended through the brass ring). Product-gas exited the furnace through a copper tube, which also passed through the brass ring

A mullite 3A crucible with inside diameter of 32 mm and outside diameter of 35 mm, and height 50 mm was used to contain the sample. (The dimensions of the crucible were chosen to ensure that the sample was representative of the bulk material[46].) The crucible, which was contained in a molybdenum basket made from 0.5mm molybdenum wire, was suspended from a scale with a molybdenum wire of 2mm diameter. The crucible was lowered into the work tube by lowering the scale (which was contained in the scale car). A DC drive was used to lower the scale.

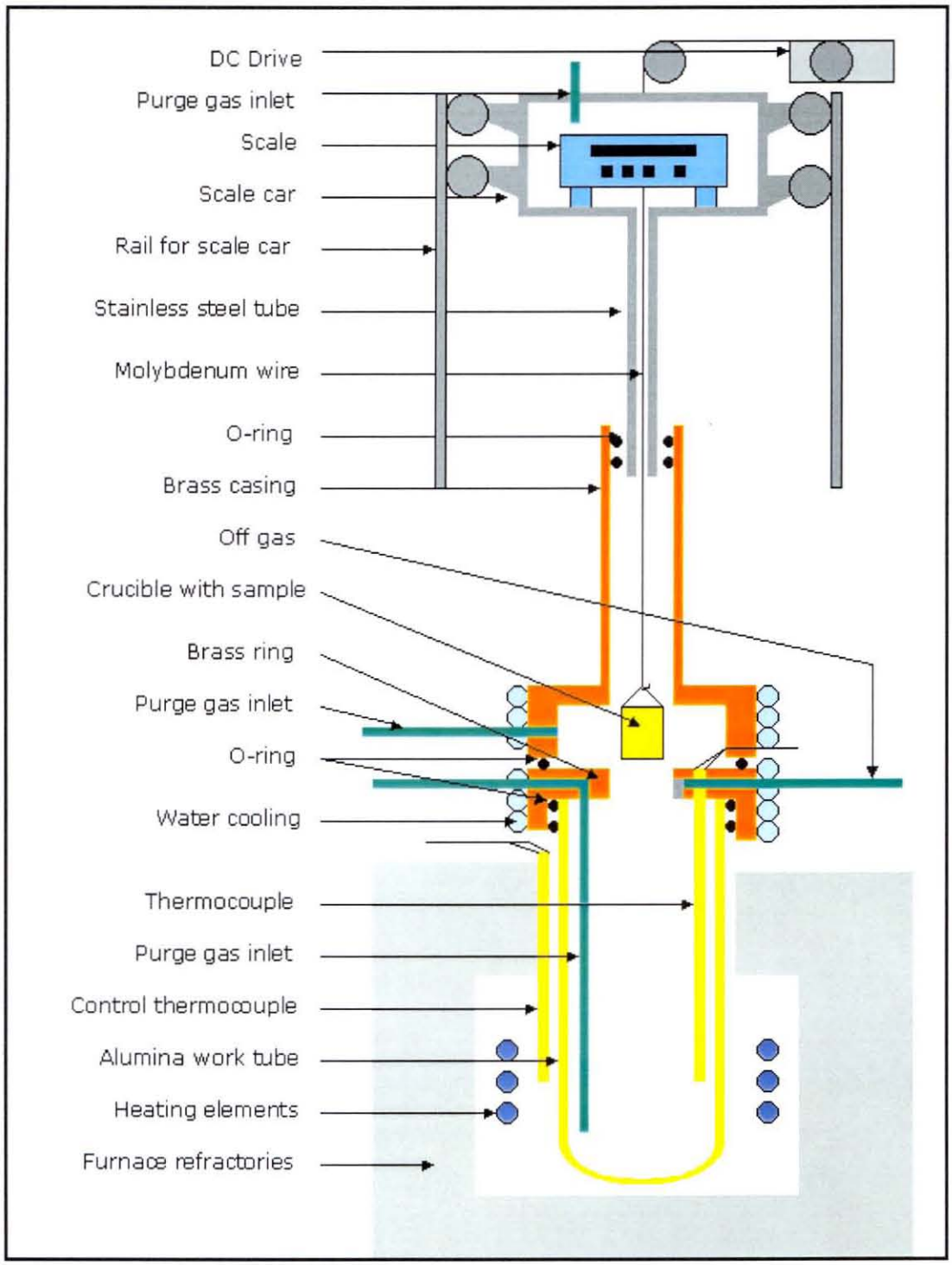

Figure 12: *Schematic illustration of the TGA furnace configuration.*

During lowering of the scale, the stainless steel tube below the scale car (of 28mm inner and 31mm outer diameter and length of 520 mm) slid into a brass casing that was clamped onto the brass ring. Two rubber O-rings and vacuum grease ensured a gas-tight seal between the stainless steel tube and brass casing. A rubber O-ring ensured a gas-tight seal between the brass casing and brass ring. The casing could be removed from the brass ring, thereby providing access to the work tube for loading and removal of samples.

2.2.1.2 Gas system

The work tube and scale car assembly was continuously purged with Argon. A schematic diagram of the gas preparation and control system, (including gas lines, purification trains, connecting gas-lines and stopcocks) is shown in ***Figure 13***.

The gas passed through Drierite ($CaSO_4$) to remove excess moisture. The argon was further purified by passing through copper turnings in a fused silica tube, which was heated to 600°C. The copper turnings have a large surface area and react with excess oxygen in the gas, to form copper oxide. The copper was periodically replaced.

From the copper turnings the gas line split into three separate gas lines. They were: a line leading to the work tube, a line to the scale car and a line to the brass casing. The gas line to the work tube was used for flushing of the tube, while the line to the brass casing was to assist with cooling of samples after testing. The gas fed to the scale car forced downward flow of gas in the stainless steel tube and brass casing, thereby protecting the scale from furnace gasses and soot. The flow rate of the argon through each line, was measured with a calibrated rotameter, thereby enabling control of the flow rate of the gas supplied to the furnace. (Calibration of rotameters are discussed in ***Appendix A.1***.) From the rotameters, the gas line led directly to the work tube, brass casing and scale car. Gas lines, which by-passed the rotameters, were included in order to flush the furnace assembly at high gas flow rates, prior to each test.

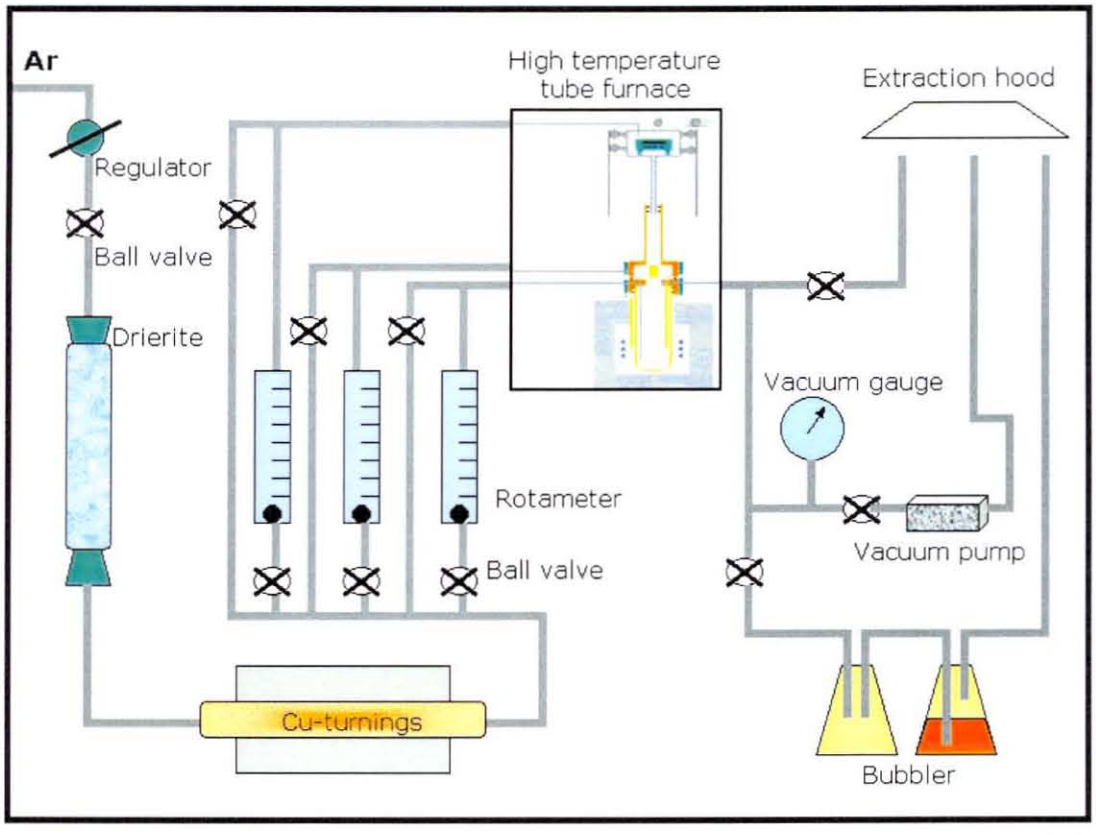

Figure 13: *Schematic illustration of the gas preparation and control system for the TGA.*

The exit gas line from the work tube was divided into three lines. One line lead to a bubbler, one to a vacuum pump and the third was a bypass, which lead directly to the extraction hood.

Oxygen entering the reaction tube assembly, could result in oxidation of species associated with the sample mass. Accordingly, leaking of air into the system had to be prevented. In addition, poisonous CO was produced during the test. All the gas that exited the system therefore had to be extracted in the gas extraction system of the laboratory for safe expulsion.

Gas-tightness of the furnace tube was checked by applying a vacuum of 15 mm Hg and noting the stability of the vacuum with time, as measured by a vacuum gauge. A significant pressure-drop in a period of two minutes indicated a leak. Serious leaks

could be found easily with a soap and water solution, but minor leaks were sometimes not traceable by this technique. A Helium snifter probe, as used in chromatography for leak detection, was obtained and minor leaks were detected by flushing and pressurising the system with helium gas and then searching along the gas-line for leaks with the snifter probe. In the event of a leakage, the relevant gas line was dismantled and reassembled.

2.2.2 Experimental procedure.

2.2.2.1 Temperature control of the heat zone

The furnace temperature was controlled by a proportional-integral-derivative (PID) controller. A Pt/Pt10%Rh (or type S) thermocouple, positioned in the hot zone of the furnace, outside the mullite work tube, served as control thermocouple (as shown in ***Figure 12***). (The method used to determine the position of the hot zone of the furnace, is discussed in ***Appendix A.2***)

The temperature inside the work tube was measured with a Pt/Pt10%Rh (or type S) thermocouple that was fixed to the brass ring, and positioned in the hot zone of the furnace at the same height as the control thermocouple. For gas-tightness, the point of entry of the thermocouple sheath into the brass ring, was sealed with silicone rubber.

A minor difference was observed between the temperature measured by the control thermocouple and the thermocouple inside the reaction tube. The difference was about 2°C at 1100°C and 4-5°C at 1400°C, with the control thermocouple reading higher then the temperature measured inside the tube. The temperature on the PID controller was therefore set at a temperature that yielded the required temperature inside the work tube.

2.2.2.2 Sample preparation

Each sample was made-up to test specific material characteristics. In order to benchmark the influence of a material characteristic on the reduction rate, a reference sample was used. The reference sample comprised of a material mixture similar to that used at the Ifcon pilot scale facility that was erected at Kumba's pilot plant. The reference sample comprised of Sishen iron ore fines, duff coal from Eikeboom collieries, dolomite from Mooiplaas and limestone from PPC lime. The

ingredients of the reference mixture are summarised in ***Table 2***. The recipe of the reference mixture was referred to as the "base mixture".

Table 2: *Ingredients of the reference mixture (base mixture recipe).*

Ore type	Mass (g)	Mass% (%)
Sishen iron ore fines	27.8	69.5
Eikeboom coal (-2mm)	7.3	18.3
Dolimite	2.2	5.5
Limestone	2.7	6.7

Raw material preparation that was done is discussed in ***Appendix A.3,*** while the chemical compositions of the various raw materials and analytical techniques used, are presented in ***Appendix A.4*** and ***Appendix A.5*** respectively.

The base mixture as well as other test mixtures were all made up in such a way that 15 grams of metal could theoretically be produced from a sample, when 80% reduction was achieved. The amount of limestone and dolomite added to each sample was such that the CaO/SiO_2 ratio of the inset material was 1.4 while the MgO content of the slag species (that remained after 80 % reduction was achieved) would be 8%. These numbers represent the characteristics of the feed mixture that was used during trails done at the Ifcon pilot plant facility. This is discussed in more detail in ***Appendix A.6.***

Material mixtures, other than the base mixture, were made up so that one material characteristic was changed for each consecutive sample. By doing this, the influence of changes to a specific material characteristic, on the degree of reduction achieved, could be determined. The degree of reduction achieved with each sample could therefore be compared to the degree of reduction achieved with the base mixture (as a function of time).

The various samples that were tested against the reference sample are listed in ***Table 3***. The changes made to material characteristics or operational conditions are also indicated in the table.

Table 3: *Experimental program that was followed to determine the influence of specific material characteristics on the reduction rate of the material mixture.*

Test no	Test objective
1	Reference samples (made up according to the "base mixture") were tested repeatedly under similar conditions to determine the repeatability of results
2	Sishen ore was replaced with Thabazimbi ore (which has a higher CO reducibility than Sishen ore) to investigate the influence of changing CO reducibility of the ore on reduction rate.
3	A mixture containing large Sishen ore particles was compared to a mixture containing smaller Sishen ore particles.
4	Eikeboom coal was replaced with Leeuwpan coal to investigate the influence of changing CO_2 reducibility of the coal
5	Coal was replaced with char to investigate the influence of volatile matter in the material mixture on the reduction rate.
6	All of the above tests were done at 1100°C and 1200°C to determine the influence of varying exposure temperature on the reduction rate.

2.2.2.3 Test procedure

Mullite crucibles (A3) were used to contain the samples. The crucible dimensions were OD 35mm, ID 32mm and height 50mm, with inner height of about 48mm. Prior to testing, the mass of each crucible was measured.

Each sample was intimately mixed, placed into a crucible, and the mass of the crucible containing the sample was measured. The crucible was placed in a basket that was made from 0.5 mm molybdenum wire, which was suspended from the scale with molybdenum wire of 2 mm diameter.

Access to the reaction tube was obtained by lifting the brass casing from the brass ring. During testing, the brass casing was fastened to the brass ring with quick-release clams. To ensure that no carbon was lost during the initial stages of the test

(due to oxidation with air), the sample was inserted into the alumina work tube at a position where the temperature in the tube was approximately 100 °C. The alumina work tube was then flushed with nitrogen for 2 minutes before the sample was lowered into the constant heat zone of the work tube.

The crucible- assembly was lowered into the work tube, by lowering the scale car with the DC drive. The crucible was lowered at such a rate that the crucible reached its final position within 10 seconds. The crucible was lowered to exactly the same height during each experiment. This was accomplished by installing a ruler next to the rail of the scale car to measure the relative height of the scale.

The alumina work tube was continuously flushed with nitrogen (at a flow rate of 0.5 litre per minute) for the duration of each experiment. The system was operated at a slight positive pressure by continuously bubbling the exiting gas through an oil trap (or bubbler).

From the moment the crucible was inserted into the furnace the mass of the crucible assembly (and therefore the rate of mass loss of the sample) was measured. Once the rate of mass loss slowed down significantly, the sample was elevated from the hot zone (into the brass ring) and left to cool to approximately 100°C (in an nitrogen atmosphere) before being removed from the work tube. Finally the mass of the crucible containing the reduced sample was measured and the total mass loss of the sample was calculated and compared to that of the reference sample. Since the analyses of the input materials were known, the apparent degree of reduction achieved for each sample was calculated as a function of time, and compared to that of the reference sample. Note that this is an apparent degree of reduction, based on assumptions made during calculations. Assumptions made during these calculations are discussed in ***Appendix A.7***.

2.3 Kinetic modelling of the TGA experiment

The model, which was developed by Pistorius *et al.*[30], was used to simulate reduction of the TGA samples. The main assumptions and calculation procedure of the model are presented below.

2.3.1 Sample configuration:

The model simulates heating of a composite sample similar to that of the TGA experiment. The samples in the TGA experiment had cylindrical shapes (with diameter of 32 mm and 45 mm high). However, in order to simplify heat transfer calculations, the samples were modelled as spheres, so that heat flux in a sample was one-dimensional towards the centre of the sample. The radius of the spherical model-samples were taken as 20 mm, so that model samples and samples that were actually tested had similar volumes.

Another advantage of modelling the samples as spheres (rather than infinitely long cylinders) is that heat entering the samples through the top and bottom sides was accounted for.

Spherical symmetry was assumed around the centre point of each sample, with the solid- and gas temperatures assumed to be the same at a given position in the sample[15,30].

Each sample was divided into ten hollow spherical nodes (except for the centre node which was a solid sphere). The thickness of each node was similar to the radius of the centre node.

The total reaction time was divided into various time steps. A mass-and energy balance was performed for each node during each time step, to yield the change in temperature of the node as a function of time.

The equilibrium constants were found from simplified expressions[15] fitted to the equilibrium constants that were calculated with the data of Kubaschewski et.al.[14]

2.3.2 Heat transfer

Since the thermal conductivity of the crucible was about 6[47] compared to a conductivity of about 1 for the sample[15], the effect of conduction through the crucible was not accounted for. Heat transfer to the sample was assumed to be by radiation only with the surface of the sample (crucible) having an emissivity of 0.8. The rate of radiation heat transfer followed the expression[30]:

$$q = \sigma \varepsilon A(T_f^4 - T_s^4) \qquad (2.q)$$

where q is the rate of heat transfer (in W), σ is the Stefan-Boltzmann constant, ε is the emissivity of the crucible (taken to be 0.8), A is the outer surface area of the sample, T_f is the furnace temperature, and Ts is the surface temperature of the crucible.

Heat transfer inside the sample occurred as conduction as well as by bulk movement of the gas[30]. For this, the effective thermal conductivity was estimated with the following relationship:

$$k_e = k_s \frac{1 - 2e(\kappa - 1)/(2\kappa + 1)}{1 + e(\kappa - 1)/(2\kappa + 1)} \qquad (2.r)$$

where e is the porosity of the sample, and $\kappa = k_s / k_g$, where k_s is the average thermal conductivity of solids in the sample, k_g is the thermal conductivity of gas in the pores, and k_e is the effective thermal conductivity of the solids bed. During each time step, the sample porosity was calculated using known densities of the species present[15]. The sizes of the nodes were assumed to remain constant with time.

The average conductivity of the solid phases in the sample was calculated, with the following geometric mean expression: [30]

$$k_s = \prod_{i=1}^{n} k_i^{f_i} \qquad (2.s)$$

where f_i is the volume fraction of the solids occupied by solid species i.

Equations and constants that were used to calculated to conductivities of the solid phases, are presented in ***Appendix B.1***.

2.3.3 Reaction rate expressions

2.3.3.1 Reduction reaction:

Stepwise reduction of hematite to magnetite, magnetite to wüstite and wustite to iron (above 564°C) or alternatively hematite to magnetite and magnetite to iron (below 564°C) was assumed. Reduction occurred by CO and H_2 in parallel. (564°C is the temperature where wustite becomes thermodynamically unstable when iron oxide is reduced with CO, assuming unit activity for all species[14].)

The reaction rates were assumed to be first-order with respect to all reactants, and the rate expressions were as follows[30]:

$$r = k_R M_{Fe} (1\text{-}F) (p_i - p_i^{equilib})/RT \qquad (2.t)$$

where r is the reduction rate (moles of O removed per unit time), k_R is the reduction rate constant (with units: $m^3\ s^{-1}\ kg^{-1}$), M_{Fe} is the mass of Fe per sample volume (with units: kg/m^3), F is the degree of reduction, p_i is the partial pressure of reductant i (H_2 or CO) (in Pa), $p_i^{equilib}$ is the equilibrium partial pressure of the reductant, R is the ideal gas constant, and T is the absolute temperature.

The rate constants were assumed to follow Arrhenius-type temperature dependences, with constants presented in ***Appendix B.1***.

2.3.3.2 Carbon gasification reaction:

Carbon gasification occurred by both the Boudouard-and the water-gas reactions. The rate of the Boudouard reaction is given by:

$$r_B = k_B M_C (p_{CO_2} - p_{CO_2}^{equilib})/RT \qquad (2.u)$$

where r_B is the Boudouard reaction rate (with units: moles of C gasified per unit time), k_B is the Boudouard reaction rate constant (with units: $m^3\ s^{-1}\ kg^{-1}$), M_C is the mass of carbon per sample volume (with units: kg/m^3), p_{CO_2} is the partial pressure of reductant CO_2 (in Pa), and $p_{CO_2}^{equilib}$ is its equilibrium partial pressure.

The water gas reaction rate is similarly given by:

$$r_{wg} = k_{Wg} M_C (p_{H_2O} - p_{H_2O}^{equilib})/RT \quad (2.v)$$

where r_{wg} is the rate of the water gas reaction (with units: moles of carbon gasified per unit time), and p_{H2O} is the partial pressure of H_2O (in Pa), and $p_{H2O}^{equilib}$ is its equilibrium partial pressure.

Expressions for equilibrium constants and enthalpies are presented in ***Appendix B.2*** and ***Appendix B.3*** respectively. Rate constants and activation energies used in the model are presented in **Appendix B.4**.

2.3.3.3 Devolatilisation

Devolatilisation was assumed to occur in two steps (in series). Each step was assumed to be first-order with respect to the amount of volatile matter remaining in the coal[15]. The rate constants and activation energies for the two steps are given in ***Appendix B.4.*** Each of the two devolatilisation steps was assumed to remove half of the volatile matter.

Default conditions for the model calculations are presented in ***Appendix B.5***.

Model predictions are presented in support of experimental results in ***Section 2.4***.

2.4 Results and discussion

2.4.1 Repeatability of results

Four tests were done with the "base mixture" to test repeatability of results. Two of the tests were done at 1100°C and two were done at 1200°C. The sample masses recorded from these tests are shown as black dotted lines in ***Figure 14***. To ensure that results were comparable, only the sample masses (excluding the masses of the crucible and crucible basket) were reported. Note that the initial masses of the base mixture samples were the same.

Figure 14 shows that the masses of the base mixture samples that were exposed to 1100°C for 20 minutes varied between 29.8 and 29.5 g, while the masses of the samples that were exposed to 1200°C for 20 minutes varied between 27.5 and 27.6 g. The variation between results from similar tests were therefore less than 5% of the difference between results from samples exposed to different conditions. This was considered repeatable enough to obtain qualitative results. The apparent degree of reduction was also calculated from these data (as shown in ***Appendix C.3 and***).

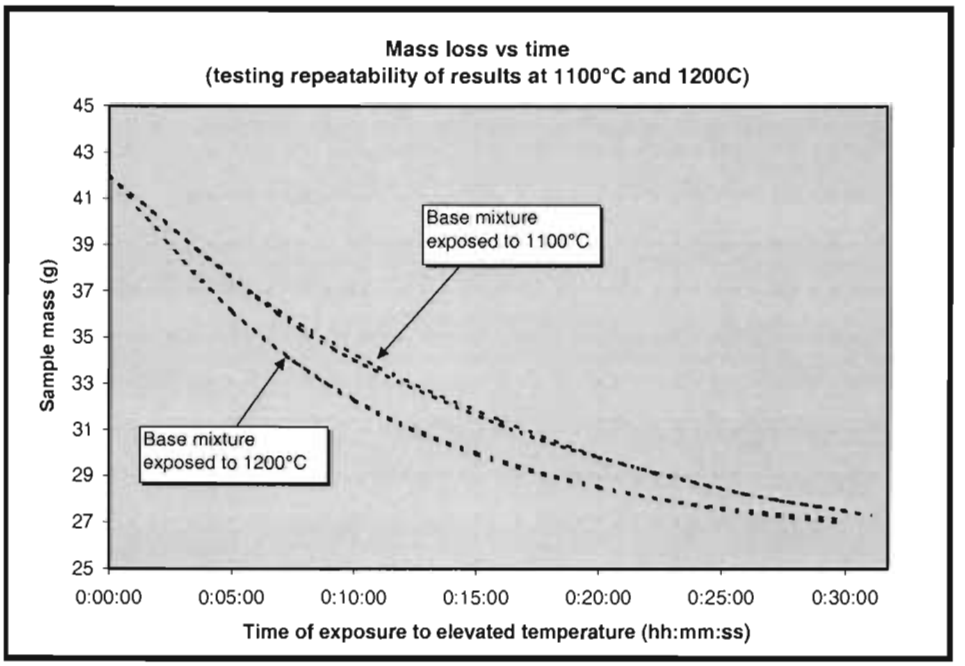

Figure 14: *Masses of base mixture samples exposure to 1100°C and 1200°C respectively as a function of exposure time, showing the repeatability of results.*

2.4.2 Influence of reducibility of ore on reduction behaviour

The model was used to predict changes to the degree of reduction when the reduction rate constant was changed. Two simulations were done: the first to establish a base line (with model inputs listed in ***Appendix B.1*** *to* ***Appendix B.5***), and the second to simulate an increase of the reduction rate constant. The reduction rate constant was increased with a factor of 10. Results are shown in ***Figure 15.***

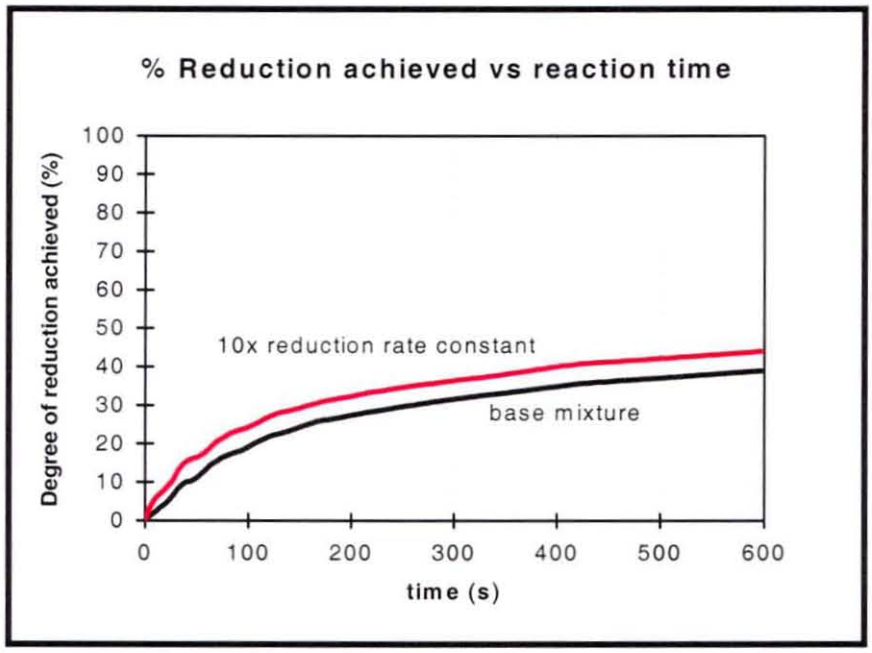

Figure 15: *Model prediction of change in degree of reduction achieved when the reduction rate constant was increased by a factor of 10. (The model prediction for the base mixture is shown as a reference (in black) with the model prediction for the increased rate constant shown in red.)*

From ***Figure 15***, it is clear that an increase in reduction rate constant, increased the degree of reduction achieved. This implies that the rate of reduction (of this specific material mixture when exposed to 1200°C) is to some extent controlled by the reduction reaction.

The extent of reduction achieved in the solids bed will therefore depend on the type of ore selected.

In order to quantify the extent to which reduction occurs (with a model), the rate constants of the ore used must be determined accurately.

The reducibility index of Sishen fine ore was reported as 1.34 percent per minute while the reducibility index for Thabazimbi fine ore was reported as about 1.49 percent per minute[48]. The rate of reduction of a material mixture containing Thabazimbi ore was therefore expected to reduce at a faster rate than the base mixture (containing Sishen ore).

When the mass loss of the mixture containing Thabazimbi ore (when exposed to 1200°C) was compared to that of the base mixture, the mass losses were similar for similar exposure times. This implies that similar reduction rates could be expected for mixtures containing Sishen ore and Thabazimbi ore. The mass vs time curves for these tests are shown in ***Figure 16.***

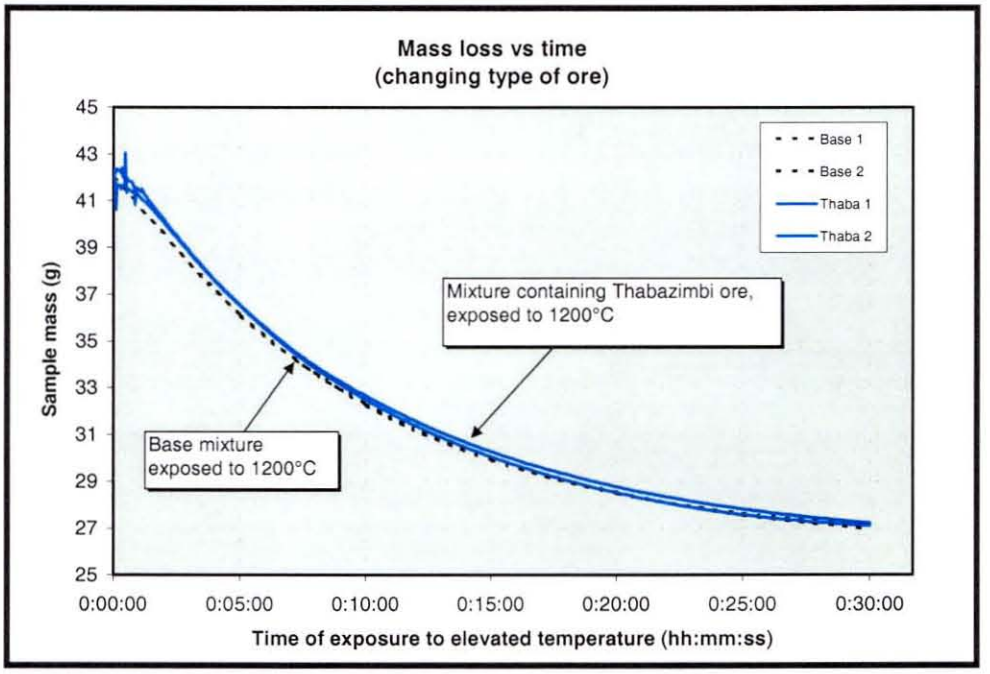

Figure 16: *Masses of base mixture samples exposure to 1200°C as well as masses of mixtures containing Thabazimbi ore exposed to 1200°C respectively, as a function of exposure time.*

The reducibility of Thabazimbi ore is about 10% higher than that of Sishen ore. To test the results, the influence of a 10% increase in the rate constant of the reduction reaction was simulated. Results (presented in **Figure 17**) showed that after 10

minutes, the mixture containing Thabazimbi ore achieved 39.3% reduction while the base mixture (containing Sishen ore) achieved 39.0% reduction. This implies that the extent to which reduction rate can be increased by increasing ore reducibility, is limited.

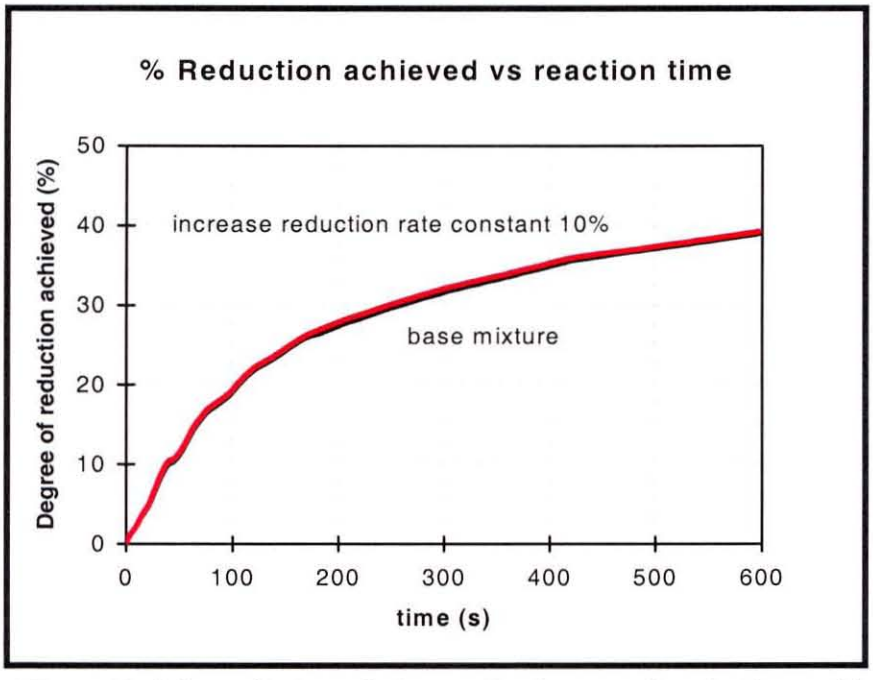

Figure 17: *Model prediction of change in degree of reduction achieved when the reduction rate constant is increased by 10%. (The model prediction for the base mixture is shown in black as a reference with the model prediction for the increased rate constant shown in red.)*

To confirm repeatability of the test, two experiments were conducted with mixtures containing Thabazimbi ore at 1100°C. ***Figure 16*** shows that the two curves obtained were similar, thereby indicating repeatability

2.4.3 Influence of ore size on reduction behaviour

Figure 18 shows the reduction rate of a material mixture containing specific size fractions, when exposed to 1200°C.

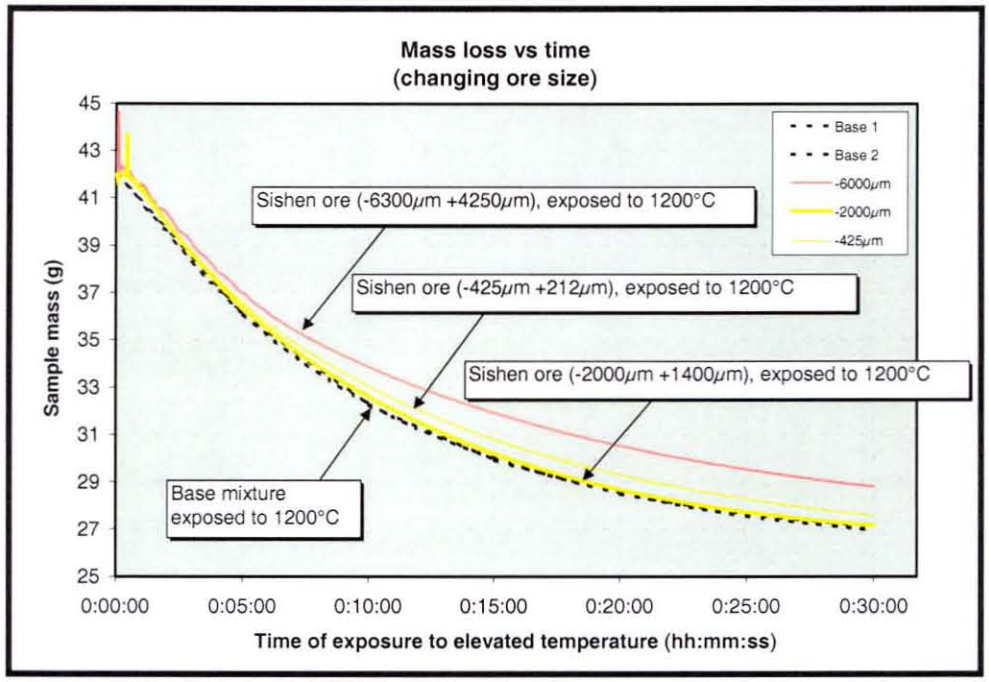

Figure 18: *Mass losses as a function of time for base mixture as well as mixtures containing various size fractions of Sishen ore during exposure to 1200°C*

Figure 18 shows that the base mixture, the mixture containing –425 +212 µm particles, and the mixture containing –2000 +1400 µm particles showed mass losses of 13.4, 13.4 and 12.7 g respectively during the first 20 minutes, while the +4750 – 6300 µm particles however only showed 11.5 g mass lost during the same time. This means that the mass loss achieved by particles smaller than 2000 µm, deviated 4.5% from the base mixture (after 20 minutes), while the +4750 µm deviated from the base mixture by 14%. From these figures it seems that the reduction rate of particles smaller than 2000µm was independent of particle size, while the reduction rate of particles larger than 4750 µm was slower. To investigate this, samples of partially reduced ore (reduced at 1200°C) was set in resin, polished and investigated with an optical microscope. (The method used for setting and polishing of the samples is similar to the procedure discussed in ***paragraph 3.4.2.2***.)

Typical images obtained are shown in **Figure 19** and **Figure 20**. **Figure 19** shows a "shrinking core" texture that was observed in some of the larger particles (+4750 µm). Most of the large particles and all of the small particles showed homogeneous reduction occurring throughout each particle. (This is shown on the right-hand-side of **Figure 20**). **Figure 20** shows two adjacent particles in the sample, one with a "shrinking core" structure and one with a homogeneous structure.

No correlation was found between the position of particles in the sample and the particle texture (shrinking core or not). This implies that the tendency of the ore particles to react according to a shrinking core, was a result of material characteristics rather than sample configuration.

From the above it was concluded that the rate of reduction in some of the larger particles (mostly larger than 4.7 mm), was controlled by the rate of diffusion of gaseous species in the particle.

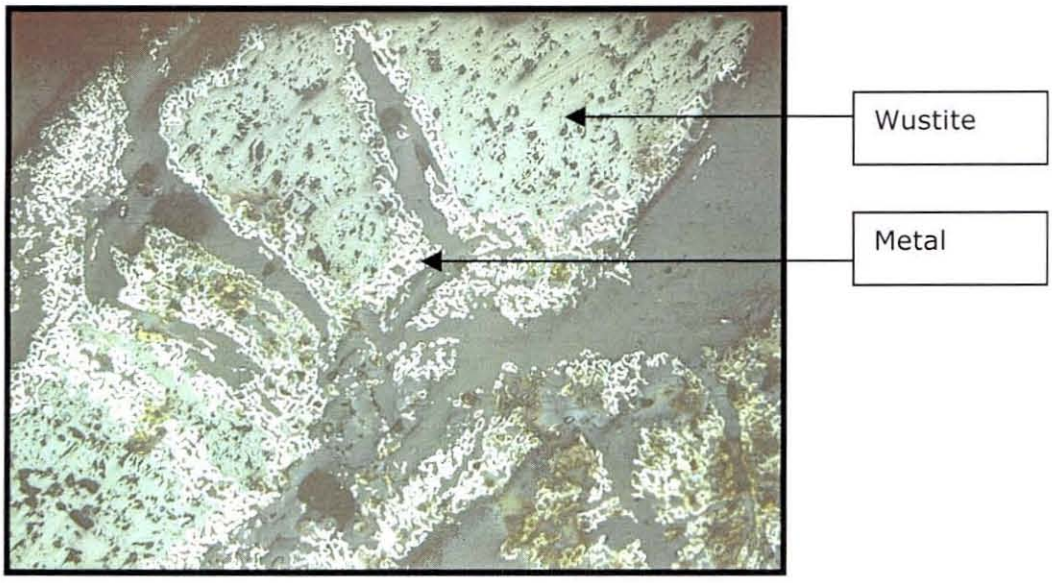

Figure 19: *Optical image of a polished section of a partially reduced +4750 µm – 6300 µm ore particle. (Width of field of view = 2 mm.)*

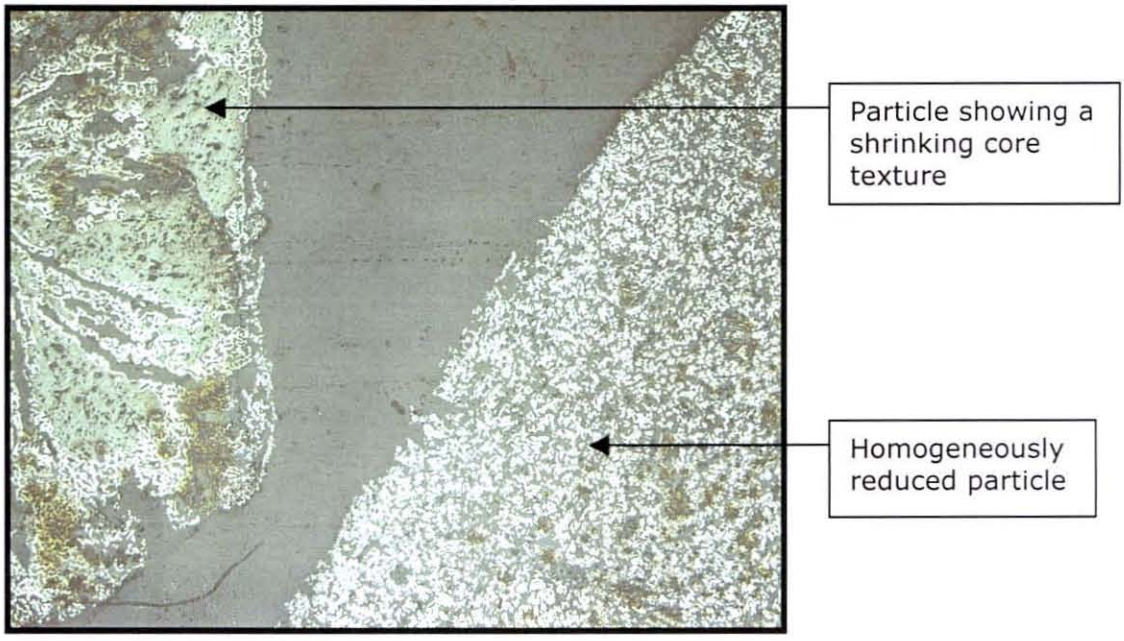

Figure 20: *Optical image of a polished section of adjacent particles that were partially reduced. (+4750 µm –6300 µm ore particle) (Width of field of view = 2 mm.)*

2.4.4 Influence of type of coal on reduction behaviour

The CO_2 reactivity of coal is the rate at which carbon in coal is oxidised by CO_2 at 1000°C. CO_2 reactivity is expressed in terms of mass of carbon reacted per unit time.

The influence of changing the CO_2 reactivity of a material mixture was modelled, by changing the rate constant for the Boudouard reaction. The results from the model are shown in ***Figure 21***.

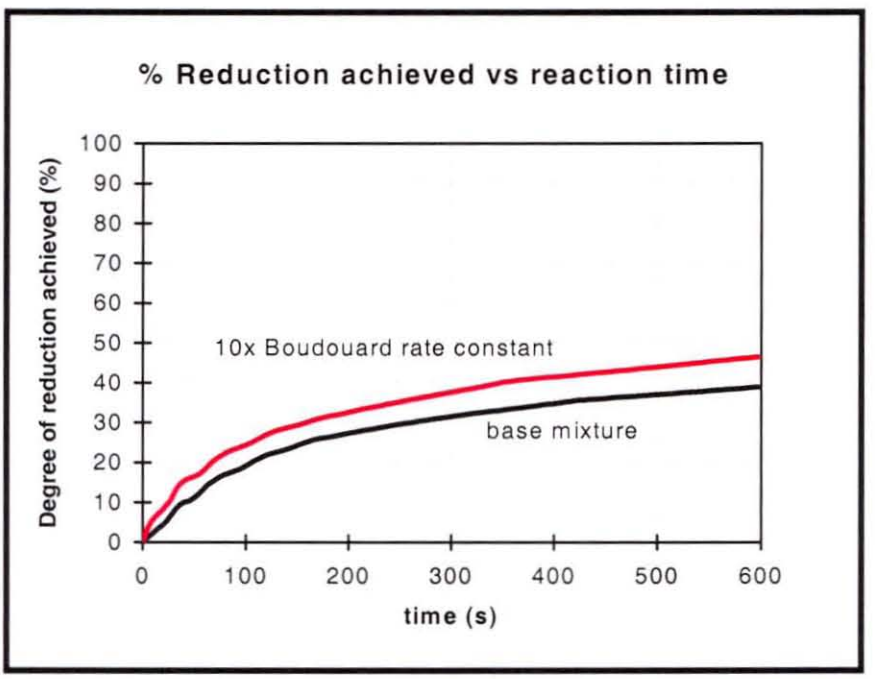

Figure 21: *Model prediction of change in degree of reduction achieved when the gasification rate constant is increased by a factor of 10. This is for a sample exposed to 1200°C. (The model prediction for the base mixture is shown as a reference (in black) while the model prediction for the increased rate constant shown in red.)*

The model results show that the degree of reduction achieved, is influenced by the CO_2 reactivity of the coal. The effect of changing the gasification reaction rate is predicted to have a similar effect as changing the rate of the reduction reaction (for this specific mixture, exposed to 1200°C).

The model predictions were experimentally tested. For the experimental investigation, Eikeboom and Leeuwpan coal, with CO_2 reactivities of 2.06 and 1.64

g/min were respectively used[48]. From the CO_2 reactivity values it can be seen that the CO_2 reactivity of the Leeuwpan coal was about 20 % higher than that of Eikeboom coal. The base mixture contained Eikeboom coal.

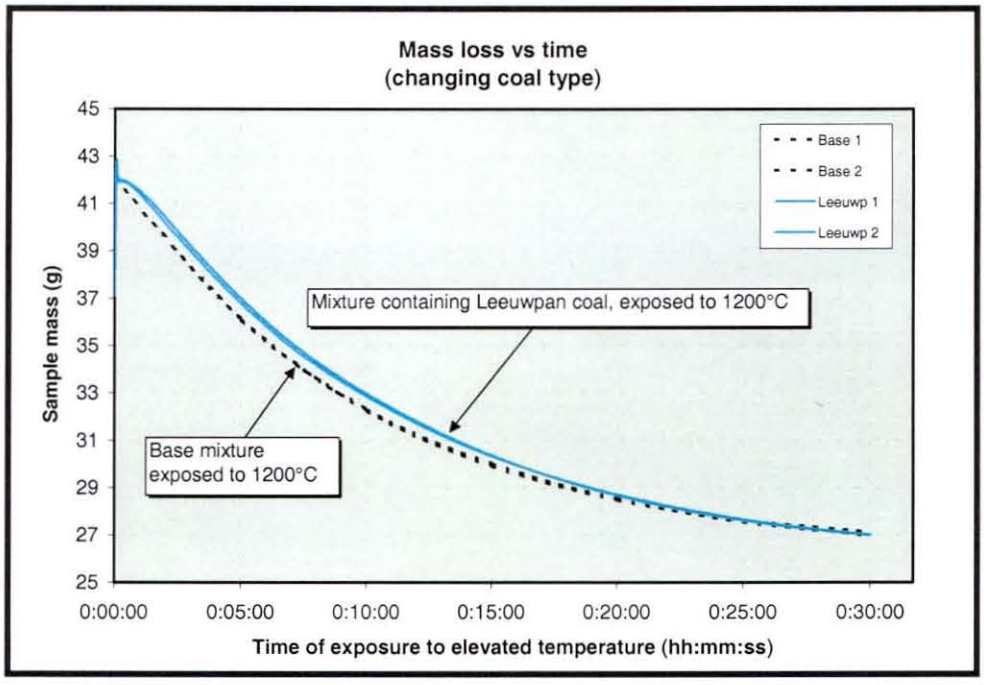

Figure 22: *Masses of base mixture samples and masses of mixtures containing Leeuwpan coal exposed to 1200°C respectively, as a function of exposure time.*

Figure 22 shows no significant change to the mass loss achieved, when the CO_2 reactivity of the material mixture changed (for exposure to 1200°C). ***Figure 22*** shows that even though the graphs in ***Figure 22*** *are* not identical, the mass loss achieved after 30 minutes of exposure was similar. Accordingly, the degree of reduction was expected to be similar. However, similar changes to the reduction rate constant and the Boudouard rate constant yielded similar changes to the overall reduction rate. This implies that the rates of the reduction- and Boudouard reaction, are similar, and the reaction may be under mixed control at some point in time. (This conclusion only holds for the specific material mixture investigated, exposed to 1200°C).

The influence of changes to the reduction and gasification rate constants on the overall reduction rate was marginal. A change in exposure temperature (as shown in ***Figure 22***) had a more prominent effect than changing rate constants.

2.4.5 Influence of amount of volatile matter of coal on reduction behaviour.

The model prediction showed that the volatile matter in coal does contribute to reduction. The presence of volatile matter increases the rate at which the composite mixture is reduced. This is shown in ***Figure 23***. Calculations were done for a furnace temperature of 1200°C.

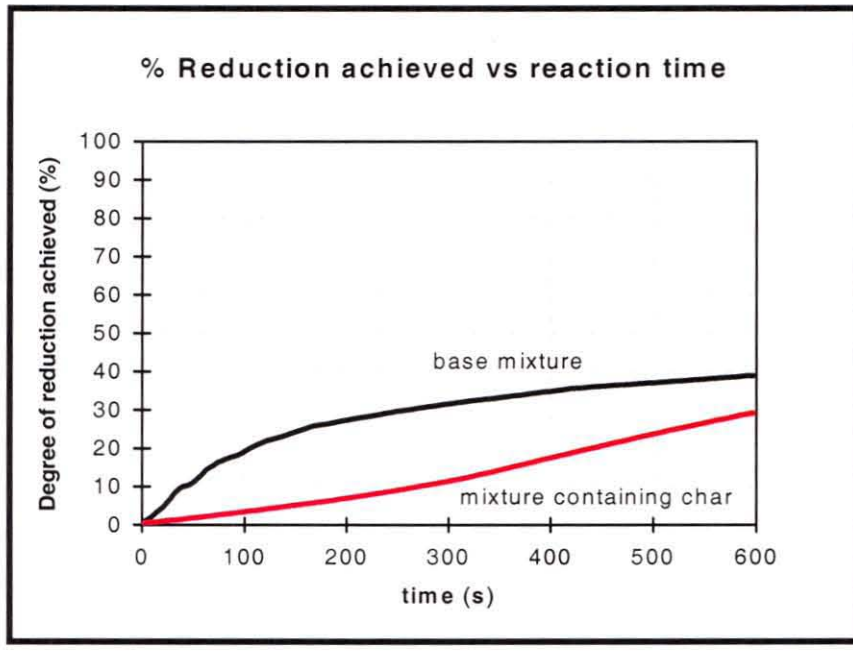

Figure 23: *Model prediction comparing the reduction rate of a mixture containing coal (with 23% volatiles) with that of a mixture containing char.*

The experimental results, shown in ***Figure 24*** (as well as ***Appendix C.2*** *and* ***Appendix C.3***), confirmed model prediction-trends. ***Figure 24*** shows that the rate at which the mass of the base mixture decreased was higher than the rate at which the mass of the sample containing coal char decreased. Although the contribution of volatile matter to the rate of reduction was not obvious from ***Figure 24***, ***Appendix C.2*** and ***Appendix C.3*** clearly show that volatile matter increased the rate of reduction. This was assumed to be a result of hydrogen reduction (noting that the rate of reduction of iron oxide with hydrogen is significantly faster than that with carbon monoxide)[50,51].

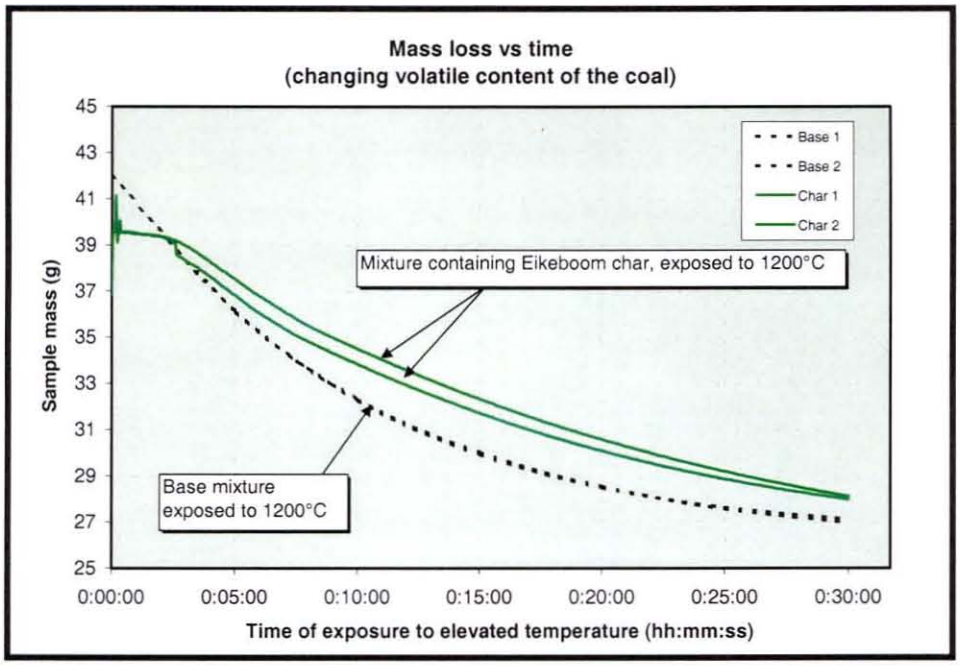

Figure 24: *Reduction rate of base mixture and a mixture containing Eikeboom char exposed to 1100°C and 1200°C respectively.*

2.4.6 Influence of exposure temperature on reduction behaviour

The model prediction showed that the rate of reduction increased when the temperature (to which the material mixture was exposed) increased. This is shown in ***Figure 25***. The model prediction was confirmed by experimental results, as shown in ***Figure 14***.

When a sample is exposed to 1200°C instead of 1100°C, the model predicted an increase from 38 to 40 % reduction (achieved after 10 minutes). Actual measurements showed that the degree of reduction that was achieved, changed from 24 to 38% (after 10 minutes exposure). Although the values were not the same, model predictions were qualitatively confirmed.

In addition, the model predictions showed that the rate of reduction increased when the conduction heat transfer coefficient increased. This implies that the rate of reduction is influenced by the rate of conduction in the material mixture. The model prediction is shown in ***Figure 26***.

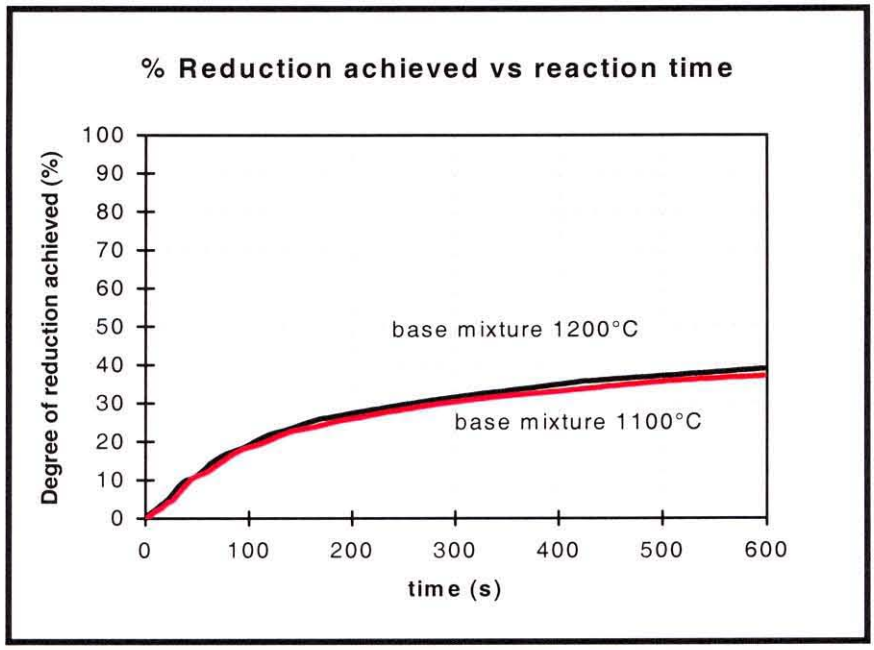

Figure 25: *Model prediction comparing the reduction rate of a mixture exposed to 1200°C to that of a mixture which was exposed to 1100°C.*

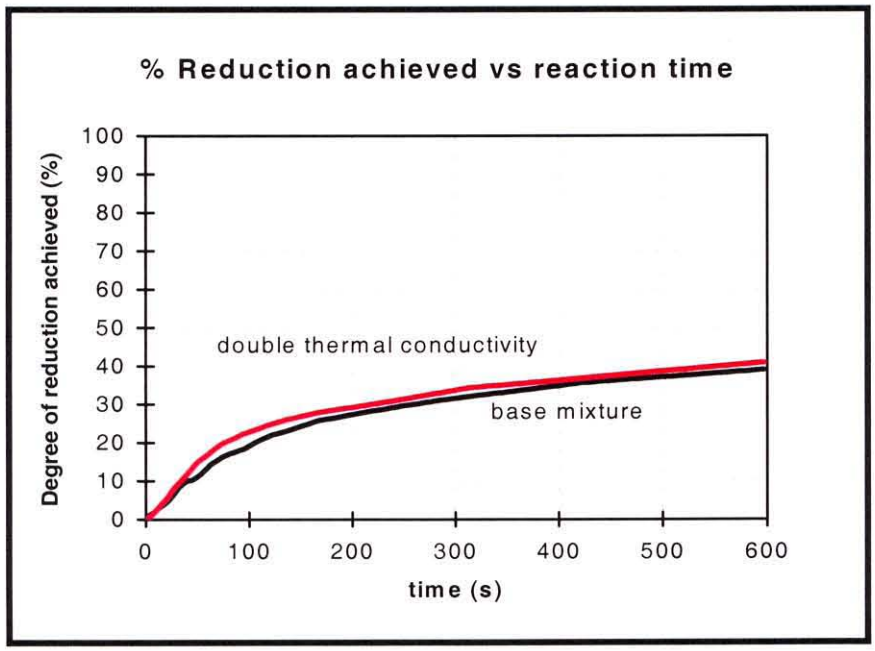

Figure 26: *Model prediction comparing the reduction rate of a base mixture to that of a mixture for which the heat transfer coefficient was doubled.*

The predicted temperature in the centre of the sample, as well as the predicted temperature of the outer surface of the sample are shown in ***Figure 27.*** This figure shows a significant temperature difference between the outer surface and the centre of the sample during the first 180 seconds of the test. The reduction occurring during this time, was therefore governed (to a great extent) by heat transfer limitations. In addition, the centre of the sample reached 700 °C after about 190 seconds. This means that there was a period at the start of each test during which the Boudouard reaction did not proceed and reduction would have been slow (especially at the centre of the sample). Actual measurements also show a period (between 240 and 360 seconds) during which reduction did not occur. (This is shown in ***Figure C.1*** *to* ***Figure C.12*** *in* ***Appendix C.2*** *and* ***Appendix C.3***.) During calculations it was however assumed that devolatilization and calcination of carbonates was completed before reduction started. This also contributed to the period of no reduction that was observed at the start of each test.

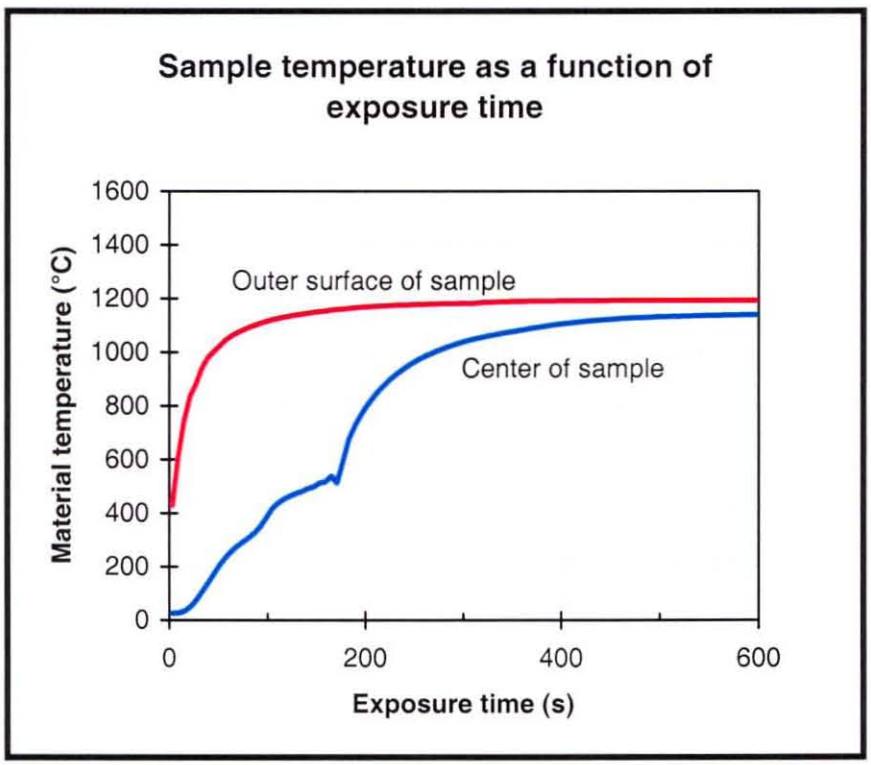

Figure 27: *Model prediction comparing the temperatures of the centre and outer surface of the sample as a function of exposure time. The centre of the sample is shown in blue, while the outer surface is shown in red.*

However, the steep temperature gradient in the sample showed that reduction was governed by the rate of heat transfer, at least during the first three minutes of each test.

2.4.7 Extent of influence of various parameters

All the tested parameters are shown on the same graph in **Figure 28.**

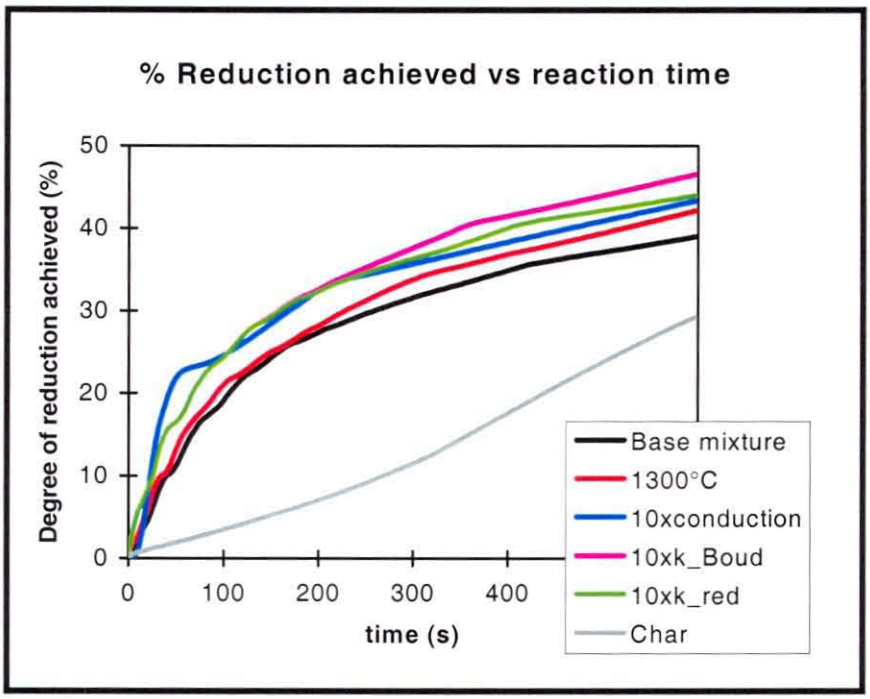

Figure 28: *Model prediction comparing the influence the exposure temperature, reduction rate constant, gasification rate constant, heat transfer coefficient and the volatile content of the material mixture on the degree of reduction achieved.*

From the graph it can be seen that increasing the exposure temperature by 100°C had a similar effect as increasing the heat transfer coefficient or rate constants by a factor of 10. The temperature to which the mixture was exposed therefore appeared to be the most significant in governing the reduction rate.

The increased reduction rate is due to better heat transfer to drive the Boudouard reaction and/or it may be due to reactions occurring faster at higher temperatures.

Volatile matter from the coal influenced the rate of reduction significantly.

The reduction rate constant, the Boudouard reaction rate constant and the conductivity of the material affected the degree of reduction achieved.

The original experimental data is presented in ***Appendix C.1***.

2.5 Conclusions

To optimise production in the solids bed of the Ifcon process, **ore and coal** should not only be selected according to chemical composition but also according to CO reducibility and CO_2 reactivity. Both of these parameters influenced the overall rate of reduction, which implies that the rates of the reduction and Boudouard reactions were of the same magnitude. The effect of changes to CO reducibility and CO_2 reactivity was however limited.

The **use of coal instead of char** increases the rate of reduction in the material mixture. This is probably due to the reduction of iron ore with hydrogen.

When the conductivity of the solids bed is increased, the extent of reduction that is achieved in the bed, also increases. This indicates that heat transfer may govern the rate of reductions (especially when the size of the sample increases). From a practical perspective, material should be fed in such a way that **conduction heat transfer is avoided**. Material will typically be fed in thin layers, so that more material is exposed to the freeboard. This will cause more heat to be transferred from the freeboard to the solids bed directly by radiation, and not via conduction through the bed material.

The degree of reduction achieved increased with increasing exposure temperature. This may be due to better heat transfer (as a result of a larger driving force for heat transfer), or it may be the result of a higher temperature region in the bed where reactions occur faster. **The temperature to which the mixture is exposed should be as high as possible**, within the limits of solid state reduction.